Revision 1

Word Count: 6715 (excluding references)

Structures and transport properties of supercritical SiO_2–H_2O and $NaAlSi_3O_8$–H_2O fluids

Yicheng Sun[1,2], Xiandong Liu[1*], and Xiancai Lu[1]

[1]State Key Laboratory for Mineral Deposits Research, School of Earth Sciences and Engineering, Nanjing University, Nanjing, Jiangsu 210023, China.

[2]Key Laboratory of Marine Hazards Forecasting, Ministry of Natural Resources, College of Oceanography, Hohai University, Nanjing, Jiangsu 210024, China.

[*] Corresponding author: Xiandong Liu (xiandongliu@nju.edu.cn)

Abstract

Speciation and transport properties of supercritical fluids is critical for understanding their behaviour in the Earth's interior. Here, we report a systematic first principles molecular dynamics simulation study of the structure, speciation, self-diffusivity (D) and viscosity (η) of SiO_2 melt, $NaAlSi_3O_8$ melt, SiO_2–H_2O and $NaAlSi_3O_8$–H_2O fluids at 2000 – 3500 K with 0 – 70 wt% H_2O. Our calculations show that as the water content increases, the proportion of Q^0 species (Q^n species, where n is the number of bridging oxygens in an individual Si/Al–O polyhedra) increases while Q^4 decreases. The proportions of Q^1, Q^2 and Q^3 species first increase and then decrease with increasing water content. The diffusivity sequence for the supercritical SiO_2–H_2O fluids is $D_H > D_O > D_{Si}$, and for the supercritical $NaAlSi_3O_8$–H_2O fluids, on the whole, is $D_{Na} \approx D_H > D_O > D_{Al} \approx D_{Si}$. The viscosities of the two systems decrease drastically at the beginning of the increase in water content, and then decrease slowly. We demonstrate that the exponential decrease in the viscosity of polymerized silicate melt with increasing water content is due to a sharp decrease in the proportion of Q^4 species and increase in Si–O–H. The typical structural feature of supercritical fluid is that it contains a large amount of easy-to-flow partially polymerized or depolymerized silicate units bonded to hydrogen, which leads to a low viscosity while being enriched in silicate. This feature provides supercritical fluids the potential to transport elements that are hard to migrate in aqueous fluids or hydrous silicate melts, such as high field strength elements.

Keywords: supercritical fluid, SiO_2-H_2O, $NaAlSi_3O_8$-H_2O, first-principles, speciation, transport properties

INTRODUCTION

Silicate melts and aqueous fluids inside the Earth play an important role in magmatism and mineralization processes. Previous studies have shown that with increasing temperature and pressure, the solubility of silicate in aqueous fluids increases, and the solubility of water in silicate melts also increases (Audétat and Keppler, 2005; Dolejs and Manning, 2010; Newton and Manning, 2008). When hydrous silicate melts are completely miscible with aqueous fluids, the phase boundary between the two liquids no longer exists and a single phase is formed (Shen and Keppler, 1997; Wang et al., 2021), i.e. supercritical geofluid, or supercritical fluid (Hermann et al., 2013; Manning, 2004; Manning, 2018; Ni et al., 2017; Shen and Keppler, 1997). Hydrous silicate melts can transport a large number of elements (Xiong et al., 2009) but may not be able to migrate over long distances due to their high viscosity. Although aqueous fluids have high mobility due to their low viscosity, they are generally considered to be too dilute resulting in a limited capacity to transport solutes (Spandler et al., 2007). Supercritical fluids not only have compositions and structures close to those of hydrous silicate melts but also have high diffusivity and low viscosity similar to aqueous fluids. Therefore, supercritical fluids have a great ability to transport elements, and thus they are thought to be a high-quality agent for mass transfer (especially for incompatible elements) in subduction zones (Chen et al., 2021; Chen et al., 2018; Ni et al., 2017; Thomas et al., 2019).

Complete miscibility between some hydrous silicate melts and aqueous fluids has been observed experimentally, and the location of the second critical endpoint has been determined for some systems. For example, the second critical endpoint of the SiO_2–H_2O system was found to be ~1353 K and 0.93 – 0.97 GPa (Hunt and Manning, 2012; Kennedy et al., 1962). Complete miscibility between hydrous silicate melt and aqueous fluid in the $NaAlSi_3O_8$–H_2O system has

been observed too, and it was found that the critical temperature decreasing with pressure, from 1262 K at 1.06 GPa to 896 K at 1.65 GPa (Shen and Keppler, 1997). After that, the second critical endpoint in the $NaAlSi_3O_8$–H_2O system was found to occur at 973 K and 1.5 GPa (Stalder et al., 2000). Recently, Makhluf et al. (2020) experimentally determined that the second critical endpoint of the $NaAlSi_3O_8$–H_2O system is at 932 K and 1.63 GPa. In addition, the second critical endpoints in the $KAlSi_3O_8$–H_2O, $SrAl_2Si_2O_8$–H_2O, peridotite–H_2O and basalt–H_2O systems were also determined (Mibe et al., 2008; Mibe et al., 2004; Mibe et al., 2007; Mibe et al., 2011). However, many basic properties are still lacking, such as microscopic structure, speciation, diffusivity, viscosity, etc. (Ni et al., 2017). To our knowledge, in terms of Si speciation, a very limited number of supercritical systems were studied (Mibe et al., 2008; Mysen, 2010; Mysen et al., 2013), and a systematic understanding is still lacking. For example, although most of Si was observed to be in the form of dimer in supercritical $KAlSi_3O_8$–H_2O fluid with a water content of 60 wt% (Mibe et al., 2008), how the speciation changes with water content remains unclear. In addition, some studies focused on the systems that are close to but still below the pressure-temperature conditions of supercritical fluids (e.g., Steele-MacInnis and Schmidt, 2014; Zotov and Keppler, 2002). In terms of viscosity, interestingly, it was found that with the increase of water content, the viscosity of albite–H_2O system decreases exponentially within the first 20 wt% H_2O but after the supercritical albite–H_2O fluid is formed, the viscosity decays almost linearly to the viscosity of pure water (Audétat and Keppler, 2004). The mechanism for this behaviour still needs more understanding. At present, it is still challenging for experiments to accurately determine the microstructure of supercritical fluids (Mibe et al., 2008) and the viscosity at high pressure and temperature (Sun et al., 2018). The lack of quantitative studies makes it impossible to establish the relationship between the microscopic

properties and its macroscopic behaviors or to draw a picture of the evolution of supercritical fluids in geological processes.

Molecular modeling is an effective method to study the properties of silicate–H_2O systems over a broad range of temperatures and pressures. But previous theoretical studies mainly focused on (hydrous) silicate melts and aqueous fluids (e.g., de Koker et al., 2013; Dingwell et al., 1998; Dingwell et al., 1996; Dufils et al., 2020; Ghosh and Karki, 2011; Gillan et al., 2016; Karki et al., 2018; Karki and Stixrude, 2010; Manning, 2018; Romano et al., 2001; Sun et al., 2020; Yang et al., 2017). So far, only one work using first-principles method to study supercritical SiO_2–H_2O fluid with 23.1 wt% H_2O has been reported (Spiekermann et al., 2016). Therefore, microscopic structure, speciation and transport properties of supercritical silicate–H_2O system are urgently needed for understanding the geological roles of supercritical fluids in the Earth's interior.

Here, we use first principles molecular dynamics method to study the structure, speciation, self-diffusivity and viscosity of SiO_2–H_2O and $NaAlSi_3O_8$–H_2O systems at 2000 – 3500 K. The evolution of these properties with increasing water content have been obtained. The transfer mechanism of H in supercritical fluids is discussed. We uncover the mechanism of the decrease in the viscosity of polymerized silicate melt with increasing water content and further discuss the effect of supercritical fluids on element migration.

COMPUTATIONAL METHODS

First principles molecular dynamics (FPMD) simulations of SiO_2–H_2O and $NaAlSi_3O_8$–H_2O systems (H_2O concentration in the range of 0 wt% – 70 wt%) were performed in the DFT code VASP (Kresse and Furthmuller, 1996a; Kresse and Furthmuller, 1996b; Kresse and Hafner, 1993;

Kresse and Hafner, 1994). The Perdew-Burke-Ernzerhof (PBE) functional (Perdew et al., 1996) was used with Grimme–D3 (i.e., PBE–D3) dispersion correction (Grimme et al., 2010). Many density functional approximations (such as PBE) do not describe long-ranged electron correlation effects well. The DFT–D3 scheme is the most commonly used method, which reproduces the inter- and intramolecular dispersion interactions reasonably (Caldeweyher et al., 2019; Grimme et al., 2010; Grimme et al., 2011). Since the systems in our study contain water, the use of PBE–D3 method is a better choice (Li et al., 2022). A plane wave cut-off of 500 ~ 520 eV and gamma point Brillouin zone sampling were used. The convergence of k-point mesh and cutoff energy were tested and found to converge the total energy to within 1 meV/atom and 3 meV/atom, respectively. The electronic self-consistency convergence criterion for the total energy was set to 10^{-5} eV. Our simulations were performed in the *NVT* ensemble with a time step of 0.5 (1.0) fs for hydrous (anhydrous) liquid. Our research focuses on the properties of supercritical fluids. For comparison, we also investigated the systems with low water content. The SiO_2–H_2O systems and $NaAlSi_3O_8$–H_2O systems contain 180–210 atoms (Table 1) and 172–316 atoms (Table 2), respectively, depending on the water content. Each SiO_2–H_2O system was first melted and equilibrated at 6000 K and then cooled to 3500 K, 3000 K and 2600 K. Each $NaAlSi_3O_8$–H_2O system was melted and cooled to 3000 K, 2500 K and 2000 K adopting the same strategy. The run durations for reaching thermal equilibrium varied from 10 ~ 20 ps. Following this, we finally performed 100-ps simulations except for the $NaAlSi_3O_8$–H_2O system with 60 wt% H_2O, which was ran for 50 ps.

For each model, we first calculated the pressure of the models under four different volumes to obtain the pressure–volume curves. Then, the volume corresponding to approximately 1 ~ 4 GPa was obtained for the simulation (Table 1 and Table 2). This puts the temperature-pressure

conditions simulated in this study above the critical curves of the SiO_2–H_2O and $NaAlSi_3O_8$–H_2O systems (Figure S1 in Supporting Information). The pressure correction for Pulay stress is included based on the method of de Koker et al. (2008). The absolute value of the Pulay correction was less than 0.2 GPa for all models. The pressure correction for PBE under binding was not applied due to lack of experimental data in the hydrous system.

The self-diffusion coefficient was calculated with the Einstein relation (Allen and Tildesley, 1989). The shear viscosity was derived from the stress autocorrelation function (ACF) over time according to the Green-Kubo relation (Allen and Tildesley, 1989). Three off-diagonal components of the stress tensor are used to calculate the shear viscosity. The pairwise radial distribution function (RDF) was used to analyze the structures. The cutoff radius used in the analysis of species is defined as the position of the first minimum in RDF. The cutoff radius is uniquely determined at each state point. The stress ACF and RDF in this study can be found in Figures S8, S9, S15 and S16 in Supporting Information.

RESULTS

Speciation and Structure

Qn Speciation. In silicate fluids, both pressure (Wang et al., 2014) and network modifiers can break the bridging oxygen (BO) bonds (Si/Al–O–Si/Al), resulting in a varying distribution of Q^n species. A Q^4 species is a Si/Al–O polyhedra with 4 BOs, and a Q^0 species is a Si/Al–O polyhedra with 0 BO (i.e., it is not attached to any other polyhedra). In most cases, Q^n notation is generally used in structures with 4 coordinated Si/Al. When the pressure increases, Si/Al can be 5-coordinate and 6-coordinate. In this case, n will be greater than 4, and Q^5 or even Q^6 will appear in the structure (Bajgain et al., 2019). In addition to pressure and network modifiers,

water can also break the Si/Al–O–Si/Al network by reacting with BO, thereby converting higher Q^n species to lower Q^n species. Q^n species provides information about local network structure in silicate fluids. As shown in Figure 1, we calculated the Q^n species for the SiO_2–H_2O systems at 2600 K, 3000 K and 3500 K, and for the $NaAlSi_3O_8$–H_2O systems at 2000 K, 2500 K and 3000 K. Our Q^0 ~ Q^4 species generally agree with those obtained in the first-principles study by Spiekermann et al. (2016) for SiO_2–H_2O system with 23.1 wt% H_2O at 3000 K (Figure 1b). In addition to Q^0 ~ Q^4 species, there was also a small amount of Q^5 species present in the systems. On the whole, the SiO_2–H_2O and $NaAlSi_3O_8$–H_2O systems show the similar distribution of Q^n species. The proportion of Q^0 increases with increasing water content while Q^4 decreases. The proportions of Q^2 and Q^3 first increase and then decrease with increasing water content. Although we only observed that the proportion of Q^1 increases first and then decreases when the water content exceeds 60 wt% at 3000 K in the SiO_2–H_2O systems (Figure 1b), it can be inferred that Q^1 will also decrease at higher water content at 2600 K and 3500 K in the SiO_2–H_2O systems. This Q^1 behaviour can also be inferred to occur in the $NaAlSi_3O_8$–H_2O systems. The maximum values for the proportions of Q^3 and Q^2 in the two systems at 3000 K occur at the positions where the water content is 20 wt% and 40 wt%, respectively. For example, in the $NaAlSi_3O_8$–H_2O systems at 3000 K, Q^3 initially increases to 37.4% as H_2O increases to 20 wt% and then decreases to 6.9% as H_2O increases to 60 wt%. Q^2 increases to 34.4% as H_2O increases to 40 wt% and then decreases. These maximum values also have the same positions in the SiO_2–H_2O systems at 2600 K and 3500 K and in the $NaAlSi_3O_8$–H_2O systems at 2000 K. But these positions are slightly different in the $NaAlSi_3O_8$–H_2O systems at 2500 K, and the maximum values for Q^3 and Q^2 occur at the positions where the water content is 10 wt% and 30 wt%, respectively. This is actually due to the water content interval that we adopted. We speculate that

the true maximum values for Q^3 and Q^2 in the SiO_2–H_2O and the $NaAlSi_3O_8$–H_2O systems occur in the range of 10–20 wt% H_2O and 30–40 wt% H_2O, respectively. The maximum value for the proportion of Q^1 probably occurs in the range of 60–70 wt% H_2O. Experimental studies on quenched hydrous [$Na_2Si_4O_9$–$Na_2(NaAl)_4O_9$] system by Mysen (2007) also found that the Q^3-abundance passes through a maximum in the 7 – 10 wt % H_2O with Al/(Al+Si) = 0.25 (Figure 1f).

Oxygen Speciation and Polymerization. As the only anion in the SiO_2–H_2O systems and the $NaAlSi_3O_8$–H_2O systems, oxygen mainly exists in the form of bridging oxygen (BO, i.e. an oxygen atom is bonded to more than one network former), nonbridging oxygen (NBO, i.e. an oxygen atom is only bonded to one network former), free oxygen (an oxygen atom is not bonded to network former or H, marked as FO), molecular H_2O (H_2O_m), free hydroxyls (OH), and H_3O (an oxygen atom is bonded to three hydrogen atoms). Both the SiO_2 melt and $NaAlSi_3O_8$ melt are fully polymerized melts, and the NBO/T (T = Si, Al) of the SiO_2–H_2O and $NaAlSi_3O_8$–H_2O systems can increase from 0 (fully polymerized) to 4 (fully depolymerized) as the water content increases. We analysed in detail the oxygen species in the two systems (Figure 2) at different temperatures with increasing water content. At 3000 K, in the SiO_2–H_2O systems, BO decreases from 99.5% to 3.6% as the water content increases from 0 wt% to 70 wt% (Figure 2a). NBO initially increases to 51.3% as the water content increases to 40 wt% and then decreases to 32.2% as the water content increases to 70 wt%. The other oxygen species (FO, OH, H_3O and H_2O_m) increase to 64.2% as the water content increases to 70 wt%. The distributions of the oxygen species at 2600 K and 3500 K are basically the same as those at 3000 K in the SiO_2–H_2O systems. These features are also found in the $NaAlSi_3O_8$–H_2O systems (Figure 2c). The initial

increase in the ratio of NBO is due to the reaction between water and BO. As more water is added, not only is more FO produced, but also the NBO ratio is correspondingly reduced. NBO/T increases almost linearly from 0.01 to 3.27 as water content increases from 0.0 wt% to 70 wt%, in the SiO_2–H_2O systems (Figure 2b). Similarly, NBO/T increases linearly from 0.09 to 2.95 as water content increases from 0.0 wt% to 60 wt%, in the $NaAlSi_3O_8$–H_2O systems (Figure 2d).

Hydrogen Speciation. Hydrogen atoms in the SiO_2–H_2O systems and the $NaAlSi_3O_8$–H_2O systems mainly exist in the form of H_2O_m and Si–O–H (one H atom is bonded to the nonbridging oxygen, marked as NBO–H). In the two systems, both H_2O_m and NBO–H species show linear changes with increasing water content at all temperatures (Figure 3). The proportion of H_2O_m species gradually increases from 6.2% to 59.4% as water content increases from 10 wt% to 70 wt%, in the SiO_2–H_2O systems at 3000 K. Correspondingly, the proportion of NBO–H species gradually decreases from 79.7% to 28.8%. In the $NaAlSi_3O_8$–H_2O systems at 3000 K, the proportion of H_2O_m species increases from 6.9% to 51.4% as water content increases from 10 wt% to 60 wt%, and the proportion of NBO–H species decreases from 66.5% to 34.5%. Interestingly, in general, both H_2O_m and NBO–H species have a negative dependence on temperature. This is due to the presence of a small number of hydrogen species that have a positive dependence on temperature in the systems (Figures S2 and S3 in Supporting Information), including free protons (H), OH, bridging –O–H–O– (HO_2), H_3O, NBO–H_2 (two hydrogen atoms are bonded to the nonbridging oxygen) and BO–H (one H atom is bonded to the bridging oxygen). Some of these species are very unstable, such as H, OH and HO_2, and in most cases they exist for less than 10

fs (Figures S4 in Supporting Information). Since the time step used for the calculation is 0.5 fs, they can be identified during the transfer of H.

Transport Properties

Diffusivities. The calculated self-diffusivities for all elements in the SiO_2–H_2O systems and the $NaAlSi_3O_8$–H_2O systems at different temperatures are shown in Figure 4 and Figure 5, respectively (the corresponding MSD can be found in Figures S5 and S6 in Supporting Information). In the SiO_2–H_2O systems at 2600 K, D_{Si} increases by two orders of magnitude as the water content increases from 10 wt% to 50 wt%. D_O and D_H increase by more than one order of magnitude. As the temperature increases to 3500 K, the increases in D_{Si}, D_O and D_H decrease with water content. This indicates that a higher temperature can weaken the enhancing effect of water on diffusivities of ions. In addition, the rate of increase in the diffusivities gradually decreases with increasing water content. The diffusivity sequence for the SiO_2–H_2O systems is $D_H > D_O > D_{Si}$. At 2600 K and 10 wt% H_2O, D_H is 33 times and 9 times higher than D_{Si} and D_O, respectively. At 3500 K and 10 wt% H_2O, D_H is 9 times and 5 times larger than D_{Si} and D_O, respectively. This shows that a higher temperature reduces the gap between D_H and D_{Si} or D_O. These phenomena are also observed in the $NaAlSi_3O_8$–H_2O systems. At 2000 K, D_{Na}, D_O and D_H increase by 3.4, 49.3 and 11.3 times, respectively, as the water content increases from 10 wt% to 50 wt%. At the same temperature, as the water content increases from 20 wt% to 50 wt%, D_{Al} and D_{Si} increase by 3.7 and 23.0 times, respectively. When the temperature rises to 3000 K, the increase in the diffusivities for all ions decreases with water content.

Viscosities. The calculated viscosities for the SiO_2–H_2O and $NaAlSi_3O_8$–H_2O systems are shown in Figure 6. Our results are consistent with the FPMD results of hydrous (with 8.25 wt% H_2O) SiO_2 liquid obtained by Karki and Stixrude (2010) and the FPMD results for the $NaAlSi_3O_8$ melt from Bajgain and Mookherjee (2020). We compared the viscosity of the $NaAlSi_3O_8$–H_2O systems with an experimental model derived from the fitting of experimental data at 873 ~ 1473 K (Audétat and Keppler, 2004). We found that the model of Audétat and Keppler (2004) can basically reproduce our viscosities at temperatures of up to 2500 K (Fig. 6b). And with increasing water content, characteristics of viscosity change obtained by Audétat and Keppler (2004) at 1073.15 K is in good agreement with our results (Figures S7 in Supporting Information). In the SiO_2–H_2O systems, the viscosity decreases by nearly 2 orders of magnitude as the water content increases from 10 wt% to 30 wt% at 2600 K (Figure 6a). At the same temperature, as the water content increases from 30 wt% to 50 wt%, the viscosity only decreases by a factor of 2. At 3000 K, the viscosity decreases exponentially in the first 40 wt% H_2O, and thereafter the change is roughly linear. A higher temperature weakens this sharp change in viscosity. At 3500 K, the viscosity basically decreases exponentially in the first 40 wt% H_2O, but the magnitude of the decrease is lower than that at lower temperatures. At a water content > 30 wt%, the viscosities of the SiO_2–H_2O systems at the three temperatures are very similar (inset of Figure 6a). When the water content exceeds 30 wt%, the viscosity approaches 0.0002 ~ 0.0008 Pa·s, that is even lower than the viscosity of liquid water (0.00089 Pa·s) under ambient pressure and temperature (Harris and Woolf, 2004). These changes in viscosity also occur in the $NaAlSi_3O_8$–H_2O systems. For example, at 3000 K, the viscosity decreases by a factor of 27 as the water content increases from 0 wt% to 30 wt%, while it only decreases by a factor of 3 from 30 wt% to 60 wt%. Similar to the SiO_2–H_2O system, the viscosities of the $NaAlSi_3O_8$–H_2O

systems at the three temperatures are very similar for water contents > 40 wt% (inset of Figure 6b).

DISCUSSION

Structures of Supercritical Fluids

A typical feature of supercritical fluids is that they are not only richer in silicates than aqueous fluids, but also maintain a low viscosity. This is mainly due to the structures of supercritical fluids. According to previous studies on the phase diagrams of the SiO_2–H_2O and $NaAlSi_3O_8$–H_2O systems (Hunt and Manning, 2012; Kennedy et al., 1962; Makhluf et al., 2020; Newton and Manning, 2008), the SiO_2–H_2O and $NaAlSi_3O_8$–H_2O systems with a water content of more than 30 wt% and 20 wt%, respectively, in this study can be regarded as supercritical fluids. In the supercritical SiO_2–H_2O and $NaAlSi_3O_8$–H_2O fluids, the proportion of Q^n species depends on the water content. When the water content is relatively low (< 50 wt%), some Q^4 still exists in the supercritical fluids. As the water content continues to increase, Q^4 decreases until it disappears completely. Corresponding to it is the continuous increase of Q^0 (Figure 1). This is because the increase in water content promotes the depolymerization of silicate, causing a transition from higher Q^n species to lower Q^n species. Steele-MacInnis and Schmidt (2014) used Raman spectroscopy to study the silicate speciation in H_2O–Na_2O–SiO_2 fluids up to 873 K and 2 GPa. They found that as the SiO_2 concentration increases to 40 mol%, the proportion of Q^0 species decreases, and the proportions of Q^1 and Q^2 increase and then decrease. In their study, the maximum values for the proportions of Q^1 and Q^2 occur in the range of 7–15 mol% SiO_2 and 20–30 mol% SiO_2, respectively (Figure S10 in Supporting Information). This is consistent with the results of our calculation. We speculate that the maximum values for the proportions of Q^1,

Q^2, and Q^3 occur in the range of 60–70 wt% H_2O, 30–40 wt% H_2O and 10–20 wt% H_2O, respectively. Experimental studies on quenched (from 1673.15 K at 1.5 GPa) hydrous Na-aluminosilicate melts also found that the Q^3-abundance passes through a maximum in the 7 – 10 wt % H_2O with Al/(Al + Si) = 0.05 – 0.25 (Figure 1f), and the position of the maximum value has a positive correlation with Al/(Al + Si) (Mysen, 2007). In addition, we find that the effect of temperature on the NBO/T and average n of Q^n for supercritical fluids is weak (Figure 2 and Figure S11 in Supporting Information). Hydrogen atoms mainly exist in the form of molecular water and NBO–H, and both of them have a negative dependence on temperature (Figure 3). The addition of water not only depolymerizes the SiO_2 and $NaAlSi_3O_8$ melts, but also converts BO into NBO–H. Yuan et al. (2020) studied the effect of water on the depolymerized Mg_2SiO_4 melt and found that with the increase of water content, the ratio of NBO–H increased linearly though NBO/T did not change much. Based on the results of this study and previous results (Mibe et al., 2008; Steele-MacInnis and Schmidt, 2014; Yuan et al., 2020), we believe that the presence of a large number of partially polymerized silicate units bonded to hydrogen is an important structural feature of supercritical fluids formed from the polymerized silicate melts (Figure 7). It can be speculated that the structural feature of supercritical fluids formed from depolymerized silicate melts is that they contain a large number of depolymerized silicate units bonded to hydrogen. Water will also bring about different changes in the viscosity of polymerized and depolymerized silicate melts, which we will discuss below.

Self-diffusion of Hydrogen in Supercritical Fluids

In supercritical fluids, the transfer mechanism of H is different under different water content. When the water content is relatively low (< 40 wt%), the transfer of H occurs mainly through the

exchange of H between NBO and NBO–H: NBO–H ... NBO → NBO ... NBO–H. This is the same as the transfer mechanism of H in hydrous silicate melt (Karki and Stixrude, 2010). When the water content is relatively high (> 60 wt%), the main transfer mechanism of H occurs not only between NBO and NBO–H, but also between NBO and H_2O_m and between different H_2O_m. In this case, a typical transfer of H is carried out like this: NBO–H … H_2O_m … H_2O_m … NBO–H → NBO … H_3O … H_2O_m … NBO–H → NBO … H_2O_m … H_3O … NBO–H → NBO … H_2O_m … H_2O_m … NBO–H_2. The free protons, free hydroxyls, H_3O, NBO–H_2, and BO–H can all play a role in the transfer of H, so we can also observe a small number of these hydrogen species in the supercritical fluids (Figures S2 and S3 in Supporting Information). The diffusivity sequence for the supercritical SiO_2–H_2O fluids is $D_H > D_O > D_{Si}$, and for the supercritical $NaAlSi_3O_8$–H_2O fluids, on the whole, is $D_{Na} \approx D_H > D_O > D_{Al} \approx D_{Si}$. Previous studies have found that in the hydrous (4.2 wt% H_2O) $NaAlSi_2O_6$ melt under low pressure (< 5 GPa), $D_H < D_{Na}$ (Bajgain et al., 2019). This is consistent with our results. When the water content is low (e.g., < 20 wt% H_2O, depending on composition and *P-T* conditions), $D_H < D_{Na}$. With the increase of water content, D_H will increase and approach or even exceed D_{Na}. This is because H mainly exists in the form of H_2O_m and NBO–H (Figure 3), and the self-diffusivity of NBO–H species is affected by Si and O. Therefore, as the water content increases, the proportion of NBO–H species decreases and the proportion of H_2O_m increases, leading to an increase in D_H that approaches or even exceeds D_{Na} at higher water content.

Viscosities

The viscosities of the silicate-H_2O systems are closely related to their structures. From the abovementioned results for the structure and transport properties, we can clearly observe the

evolution of these properties for the silicate-H_2O systems as the water content increases. For the fully polymerized silicate melts, both silica and albite melts react with water and rapidly decompose: Si–O–Si + H_2O → 2Si–OH. The bridging oxygen in the silicate melt is transformed into nonbridging oxygen (Figure 2). As the water content increases, the higher Q^n species transition to the lower Q^n species during dissolution: $Q^4 \rightarrow Q^3 \rightarrow Q^2 \rightarrow Q^1 \rightarrow Q^0$ (Figure 1). This process results in a decrease in viscosity and an increase in diffusivity. In the SiO_2–H_2O systems, the viscosity decreases drastically in the first 30 wt% H_2O at 2600 K, and thereafter, the change is slow. At 3000 K and 3500 K, a sharp drop in the viscosity occurs roughly in the first 40 wt% H_2O. This corresponds to the sharp drop in the proportion of Q^4 species in the first 30 ~ 40 wt% H_2O. As the water content increases to 30 wt% (2600 K), 40 wt% (3000 K) and 40 wt% (3500 K), the proportion of Q^4 species decreases to 8.0%, 3.2%, and 3.9%, respectively. This has also been observed in the $NaAlSi_3O_8$–H_2O systems. The viscosity in the $NaAlSi_3O_8$–H_2O systems decreases drastically in the first 40 wt% H_2O, and thereafter the change is slow (inset of Figure 6b). When the water content increases to 40 wt%, the proportion of Q^4 species at 2000 K, 2500 K and 3000 K decreases to 8.1%, 4.9% and 5.9%, respectively. At low water content, H_2O_m dissolves into the melts to form Si–OH and gradually breaks the network structure of the polymerized silicate melts until Q^4 is almost exhausted. This leads to a sharp drop in the viscosity. As the water content further increases, the silicate solute continues to depolymerize, that is, $Q^3 \rightarrow Q^2 \rightarrow Q^1 \rightarrow Q^0$, while the viscosity of the silicate–H_2O systems decreases slowly. Due to the continuous increase in molecular water in the systems, the viscosity tends to get close to the viscosity of water. The decomposition of the Q^4 species means that the three-dimensional network structure of the polymerized silicate melts is destroyed, creating easy-to-flow partially polymerized silicate units (Bockris et al., 1955; Steele-MacInnis and Schmidt, 2014). Yuan et al.

(2020) found that both the ratio of NBO–H and the self-diffusion coefficient increased linearly as the water content increased from 0.0 wt% to 26.7 wt%. From the Eyring relation (Eyring, 1982), it can be speculated that the viscosity will also decrease linearly. This shows that a correlation exists between NBO–H and self-diffusion coefficient/viscosity, that is linear at least for the water content < 30 wt%. Why does the viscosity decrease exponentially in the SiO_2–H_2O and the $NaAlSi_3O_8$–H_2O systems? The same phenomenon was observed in the experimental study of the $NaAlSi_3O_8$–H_2O systems (Figure 6b) by Audétat and Keppler (2004). Here we can conclude that the reason is that the water not only generates a large amount of NBO–H, but also converts higher Q^n species to lower Q^n species, i.e. breaking the network structure in the polymerized silicate melts. Therefore, in the SiO_2–H_2O and $NaAlSi_3O_8$–H_2O systems, the superposition of these two effects leads to a sharp decrease in viscosity when Q^4 species decreases sharply.

IMPLICATIONS

The structures and transport properties of supercritical fluids are key to understanding the role they play in mineralization processes at subduction zones. The speciation and transport properties of the SiO_2–H_2O and $NaAlSi_3O_8$–H_2O systems can reflect the characteristics of the silicate–H_2O system with NBO/T < 1 such as basaltic and picritic melts. Our results show that in supercritical fluids with high water content (> 60 wt% H_2O), network-forming elements mainly exists in the form of Q^0, Q^1 and Q^2 species. While in the supercritical fluids with low water content (< 40 wt% H_2O), network-forming elements are mainly distributed in the forms of Q^1, Q^2 and Q^3 species (Figure 1). If the supercritical fluids are formed from depolymerized silicate melts, their structures are dominated by Q^0. Such Q^n distribution keeps the supercritical fluid rich in silicate and at the same time makes the fluid have partially polymerized structures and thus

low viscosity and high diffusivity. Therefore, supercritical fluids can transport elements that are hard to migrate in aqueous fluids (such as high field strength elements). The transport of dissolved species in supercritical fluids is determined by the transport properties and the solubility of the species involved. Audétat and Keppler (2004) found that the viscosities of supercritical fluids with different compositions at similar temperature and pressure are very close when measuring the viscosities of albite–H_2O systems, leucite–H_2O systems and pectolite–H_2O systems. Our results also show that when the water content exceeds 20 wt%, the viscosities of the SiO_2–H_2O systems at 3000 K are very similar to those of the $NaAlSi_3O_8$–H_2O systems at the same temperature (Figure S12 in Supporting Information). Although the pressures of the two systems are not exactly the same, a pressure difference of less than 1 GPa has a weak effect on the viscosity under high temperature conditions (Bajgain and Mookherjee, 2020; Karki et al., 2011). Therefore, the viscosity of supercritical fluids with different compositions at the same temperature and pressure may be similar. If this is the case, the element transport ability of supercritical fluids in the Earth's interior may depend more on the solubility of that element. This problem still needs more research (especially supercritical fluids with different compositions) to confirm.

The next question to be solved is how do supercritical fluids transport elements that are hard to migrate in aqueous fluids? Our research indicate that the supercritical fluids have such potential, but the complexations of these elements in the supercritical fluids remain unclear. The self-diffusion coefficients of elements in the SiO_2–H_2O and the $NaAlSi_3O_8$–H_2O systems are given in this work. Combining these data with future self-diffusion data at low temperatures obtained through experiments or simulations, a diffusion model for supercritical fluids can be

established. According to this model, we can infer the migration rate of supercritical fluid to various elements under different conditions.

ACKNOWLEDGMENTS AND FUNDING

This work was supported by the National Key R&D Program of China (No. 2018YFA0702700), the National Natural Science Foundation of China (Nos. 42003048, 41872041). We are grateful to the High-Performance Computing Center (HPCC) of Nanjing University for performing the simulations in this paper using its blade cluster system.

REFERENCES CITED

Allen, M.P., and Tildesley, D.J. (1989) Computer simulation of liquids. 385 p. Oxford University Press, New York.

Audétat, A., and Keppler, H. (2004) Viscosity of fluids in subduction zones. Science, 303(5657), 513-516.

—— (2005) Solubility of rutile in subduction zone fluids, as determined by experiments in the hydrothermal diamond anvil cell. Earth and Planetary Science Letters, 232(3), 393-402.

Bajgain, S.K., and Mookherjee, M. (2020) Structure and properties of albite melt at high pressures. Acs Earth and Space Chemistry, 4(1), 1-13.

Bajgain, S.K., Peng, Y., Mookherjee, M., Jing, Z.C., and Solomon, M. (2019) Properties of Hydrous Aluminosilicate Melts at High Pressures. Acs Earth and Space Chemistry, 3(3), 390-402.

Bockris, J.O., Mackenzie, J.D., and Kitchener, J.A. (1955) Viscous flow in silica and binary liquid silicates. Transactions of the Faraday Society, 51(12), 1734-1748.

Caldeweyher, E., Ehlert, S., Hansen, A., Neugebauer, H., Spicher, S., Bannwarth, C., and Grimme, S. (2019) A generally applicable atomic-charge dependent London dispersion correction. Journal of Chemical Physics, 150(15), 154122.

Chen, W., Xiong, X.L., and Takahashi, E. (2021) Zircon solubility in solute-rich supercritical fluids and Zr transfer from slab to wedge in the deep subduction process. Journal of Geophysical Research: Solid Earth, 126(9), e2021JB021970.

Chen, W., Xiong, X.L., Wang, J.T., Xue, S., Li, L., Liu, X.C., Ding, X., and Song, M.S. (2018) TiO_2 solubility and Nb and Ta partitioning in rutile-silica-rich supercritical fluid systems: Implications for subduction zone processes. Journal of Geophysical Research: Solid Earth, 123(6), 4765-4782.

de Koker, N., Karki, B.B., and Stixrude, L. (2013) Thermodynamics of the MgO-SiO_2 liquid system in Earth's lowermost mantle from first principles. Earth and Planetary Science Letters, 361, 58-63.

de Koker, N.P., Stixrude, L., and Karki, B.B. (2008) Thermodynamics, structure, dynamics, and freezing of Mg_2SiO_4 liquid at high pressure. Geochimica et Cosmochimica Acta, 72(5), 1427-1441.

Dingwell, D.B., Hess, K.U., and Romano, C. (1998) Viscosity data for hydrous peraluminous granitic melts: Comparison with a metaluminous model. American Mineralogist, 83(3-4), 236-239.

Dingwell, D.B., Romano, C., and Hess, K.U. (1996) The effect of water on the viscosity of a haplogranitic melt under P-T-X conditions relevant to silicic volcanism. Contributions to Mineralogy and Petrology, 124(1), 19-28.

Dolejs, D., and Manning, C.E. (2010) Thermodynamic model for mineral solubility in aqueous fluids: theory, calibration and application to model fluid-flow systems. Geofluids, 10(1-2), 20-40.

Dufils, T., Sator, N., and Guillot, B. (2020) A comprehensive molecular dynamics simulation study of hydrous magmatic liquids. Chemical Geology, 533, 119300.

Eyring, H. (1982) Statistical mechanics and dynamics. Wiley, New York.

Flyvbjerg, H., and Petersen, H.G. (1989) Error-estimates on averages of correlated data. Journal of Chemical Physics, 91(1), 461-466.

Ghosh, D.B., and Karki, B.B. (2011) Diffusion and viscosity of Mg_2SiO_4 liquid at high pressure from first-principles simulations. Geochimica et Cosmochimica Acta, 75(16), 4591-4600.

Gillan, M.J., Alfe, D., and Michaelides, A. (2016) Perspective: How good is DFT for water? Journal of Chemical Physics, 144(13).

Grimme, S., Antony, J., Ehrlich, S., and Krieg, H. (2010) A consistent and accurate ab initio parametrization of density functional dispersion correction (DFT-D) for the 94 elements H-Pu. Journal of Chemical Physics, 132(15).

Grimme, S., Ehrlich, S., and Goerigk, L. (2011) Effect of the damping function in dispersion corrected density functional theory. Journal of Computational Chemistry, 32(7), 1456-1465.

Harris, K.R., and Woolf, L.A. (2004) Temperature and volume dependence of the viscosity of water and heavy water at low temperatures. Journal of Chemical and Engineering Data, 49(4), 1064-1069.

Hermann, J., Zheng, Y.-F., and Rubatto, D. (2013) Deep fluids in subducted continental crust. Elements, 9(4), 281-287.

Hunt, J.D., and Manning, C.E. (2012) A thermodynamic model for the system SiO_2-H_2O near the upper critical end point based on quartz solubility experiments at 500-1100 °C and 5-20 kbar. Geochimica et Cosmochimica Acta, 86, 196-213.

Karki, B.B., Bohara, B., and Stixrude, L. (2011) First-principles study of diffusion and viscosity of anorthite ($CaAl_2Si_2O_8$) liquid at high pressure. American Mineralogist, 96(5-6), 744-751.

Karki, B.B., Ghosh, D.B., and Bajgain, S.K. (2018) Simulation of silicate melts under pressure. In Y. Kono, and C. Sanloup, Eds. Magmas Under Pressure: Advances in High-Pressure Experiments on Structure and Properties of Melts, p. 419-453. Elsevier.

Karki, B.B., and Stixrude, L.P. (2010) First-principles study of enhancement of transport properties of silica melt by water. Physical Review Letters, 104(21).

Kennedy, G.C., Wasserburg, G.J., Heard, H.C., and Newton, R.C. (1962) The upper three-phase region in the system SiO_2-H_2O. American Journal of Science, 260(7), 501-521.

Kobsch, A., and Caracas, R. (2020) The critical point and the supercritical state of alkali feldspars: Implications for the behavior of the crust during impacts. Journal of Geophysical Research: Planets, 125(9), e2020JE006412.

Kresse, G., and Furthmuller, J. (1996a) Efficiency of ab-initio total energy calculations for metals and semiconductors using a plane-wave basis set. Computational Materials Science, 6(1), 15-50.

—— (1996b) Efficient iterative schemes for ab initio total-energy calculations using a plane-wave basis set. Physical Review B, 54(16), 11169-11186.

Kresse, G., and Hafner, J. (1993) Ab initio molecular dynamics for liquid metals. Physical Review B, 47(1), 558-561.

—— (1994) Ab initio molecular-dynamics simulation of the liquid-metal-amorphous-semiconductor transition in germanium. Physical Review B, 49(20), 14251-14269.

Li, Y., Pan, H., Liu, Q., Ming, X., and Li, Z. (2022) Ab initio mechanism revealing for tricalcium silicate dissolution. Nature Communications, 13(1), 1253.

Makhluf, A.R., Newton, R.C., and Manning, C.E. (2020) Experimental investigation of phase relations in the system $NaAlSi_3O_8$-H_2O at high temperatures and pressures: liquidus

relations, liquid-vapor mixing, and critical phenomena at deep crust-upper mantle conditions. Contributions to Mineralogy and Petrology, 175(8).

Manning, C.E. (2004) The chemistry of subduction-zone fluids. Earth and Planetary Science Letters, 223(1-2), 1-16.

—— (2018) Fluids of the lower crust: Deep is different. Annual Review of Earth and Planetary Sciences, 46, 67-97.

Mibe, K., Chou, I.M., and Bassett, W.A. (2008) In situ Raman spectroscopic investigation of the structure of subduction-zone fluids. Journal of Geophysical Research: Solid Earth, 113(B4).

Mibe, K., Kanzaki, M., Kawamoto, T., Matsukage, K.N., Fei, Y.W., and Ono, S. (2004) Determination of the second critical end point in silicate-H_2O systems using high-pressure and high-temperature X-ray radiography. Geochimica et Cosmochimica Acta, 68(24), 5189-5195.

—— (2007) Second critical endpoint in the peridotite-H_2O system. Journal of Geophysical Research: Solid Earth, 112(B3), 8.

Mibe, K., Kawamoto, T., Matsukage, K.N., Fei, Y.W., and Ono, S. (2011) Slab melting versus slab dehydration in subduction-zone magmatism. Proceedings of the National Academy of Sciences of the United States of America, 108(20), 8177-8182.

Momma, K., and Izumi, F. (2011) VESTA 3 for three-dimensional visualization of crystal, volumetric and morphology data. Journal of Applied Crystallography, 44, 1272-1276.

Mysen, B. (2010) Structure of H_2O-saturated peralkaline aluminosilicate melt and coexisting aluminosilicate-saturated aqueous fluid determined in-situ to 800 °C and 800 MPa. Geochimica et Cosmochimica Acta, 74(14), 4123-4139.

Mysen, B.O. (2007) The solution behavior of H_2O in peralkaline aluminosilicate melts at high pressure with implications for properties of hydrous melts. Geochimica et Cosmochimica Acta, 71(7), 1820-1834.

Mysen, B.O., Mibe, K., Chou, I.M., and Bassett, W.A. (2013) Structure and equilibria among silicate species in aqueous fluids in the upper mantle: Experimental SiO2-H_2O and MgO-SiO_2-H_2O data recorded in situ to 900 °C and 5.4 GPa. Journal of Geophysical Research: Solid Earth, 118(12), 6076-6085.

Newton, R.C., and Manning, C.E. (2008) Thermodynamics of SiO_2-H_2O fluid near the upper critical end point from quartz solubility measurements at 10 kbar. Earth and Planetary Science Letters, 274(1-2), 241-249.

Ni, H.W., Zhang, L., Xiong, X.L., Mao, Z., and Wang, J.Y. (2017) Supercritical fluids at subduction zones: Evidence, formation condition, and physicochemical properties. Earth-Science Reviews, 167, 62-71.

Perdew, J.P., Burke, K., and Ernzerhof, M. (1996) Generalized gradient approximation made simple. Physical Review Letters, 77(18), 3865-3868.

Romano, C., Poe, B., Mincione, V., Hess, K.U., and Dingwell, D.B. (2001) The viscosities of dry and hydrous $XAlSi_3O_8$ (X = Li, Na, K, $Ca_{0.5}$, $Mg_{0.5}$) melts. Chemical Geology, 174(1-3), 115-132.

Shen, A.H., and Keppler, H. (1997) Direct observation of complete miscibility in the albite–H_2O system. Nature, 385(6618), 710-712.

Spandler, C., Mavrogenes, J., and Hermann, J. (2007) Experimental constraints on element mobility from subducted sediments using high-P synthetic fluid/melt inclusions. Chemical Geology, 239(3-4), 228-249.

Spiekermann, G., Wilke, M., and Jahn, S. (2016) Structural and dynamical properties of supercritical H_2O-SiO_2 fluids studied by ab initio molecular dynamics. Chemical Geology, 426, 85-94.

Stalder, R., Ulmer, P., Thompson, A.B., and Gunther, D. (2000) Experimental approach to constrain second critical end points in fluid/silicate systems: Near-solidus fluids and melts in the system albite-H_2O. American Mineralogist, 85(1), 68-77.

Steele-MacInnis, M., and Schmidt, C. (2014) Silicate speciation in H_2O-Na_2O-SiO_2 fluids from 3 to 40 mol% SiO_2, to 600 °C and 2 GPa. Geochimica et Cosmochimica Acta, 136, 126-141.

Sun, Y., Zhou, H., Liu, X., Yin, K., and Lu, X. (2020) Physical state of an early magma ocean constrained by the thermodynamics and viscosity of iron silicate liquid. Earth and Planetary Science Letters, 551, 116556.

Sun, Y., Zhou, H., Yin, K., Zhao, M., Xu, S., and Lu, X. (2018) Transport properties of Fe_2SiO_4 melt at high pressure from classical molecular dynamics: Implications for the lifetime of the magma ocean. Journal of Geophysical Research: Solid Earth, 123(5), 3667-3679.

Thomas, R., Davidson, P., and Appel, K. (2019) The enhanced element enrichment in the supercritical states of granite–pegmatite systems. Acta Geochimica, 38(3), 335-349.

Wang, Q.X., Zhou, D.Y., Li, W.C., and Ni, H.W. (2021) Spinodal decomposition of supercritical fluid forms melt network in a silicate-H2O system. Geochemical Perspectives Letters, 18, 22-26.

Wang, Y., Sakamaki, T., Skinner, L.B., Jing, Z., Yu, T., Kono, Y., Park, C., Shen, G., Rivers, M.L., and Sutton, S.R. (2014) Atomistic insight into viscosity and density of silicate melts under pressure. Nature Communications, 5(1), 3241.

Xiong, X.L., Keppler, H., Audetat, A., Gudfinnsson, G., Sun, W.D., Song, M.S., Xiao, W.S., and Yuan, L. (2009) Experimental constraints on rutile saturation during partial melting of

metabasalt at the amphibolite to eclogite transition, with applications to TTG genesis. American Mineralogist, 94(8-9), 1175-1186.

Yang, F., Hess, K.U., Unruh, T., Mamontov, E., Dingwell, D.B., and Meyer, A. (2017) Intrinsic proton dynamics in hydrous silicate melts as seen by quasielastic neutron scattering at elevated temperature and pressure. Chemical Geology, 461, 152-159.

Yuan, L., Steinle-Neumann, G., and Suzuki, A. (2020) Structure and density of H_2O-rich Mg_2SiO_4 melts at high pressure from ab initio simulations. Journal of Geophysical Research: Solid Earth, 125(10), e2020JB020365.

Zotov, N., and Keppler, H. (2002) Silica speciation in aqueous fluids at high pressures and high temperatures. Chemical Geology, 184(1-2), 71-82.

FIGURE CAPTIONS

Figure 1. Fraction of Q^n species in the SiO_2–H_2O systems and the $NaAlSi_3O_8$–H_2O systems at different temperatures as a function of water content. The green curves represent the average n for Q^n species, and the values correspond to the right y-axis in green. The filled triangles in (**b**) are the calculated Q^0, Q^1, Q^2, Q^3 and Q^4 species (legend in the same color) in the SiO_2–H_2O system with 23.1 wt% H_2O at 3000 K (Spiekermann et al., 2016), and the average n for Q^n is shown by green filled diamond. The dashed curves in (**f**) represent the experimental Q^1, Q^2, Q^3 and Q^4 species in the hydrous [$Na_2Si_4O_9$–$Na_2(NaAl)_4O_9$] system with Al/(Al+Si) = 0.25 (Mysen, 2007). The filled triangles in (**f**) are the FPMD results of anhydrous (2.28 GPa) and hydrous (4.2 wt% H_2O, 2.03 GPa) $NaAlSi_2O_6$ melt at 3000 K (Bajgain et al., 2019).

Figure 2. Oxygen speciation and (oxygen species)/T with increasing water content. (**a**) Oxygen speciation in the SiO_2–H_2O systems at 2600 K (blue symbols), 3000 K (red symbols) and 3500 K (green symbols). The squares, diamonds and circles represent bridging oxygen (BO), nonbridging oxygen (NBO) and other oxygen species (FO, OH, H_3O, and H_2O_m), respectively.

(**b**) NBO/T in the SiO_2–H_2O systems. (**c**) Oxygen speciation in the $NaAlSi_3O_8$–H_2O systems at 2000 K (yellow symbols), 2500 K (blue symbols) and 3000 K (red symbols). (**d**) NBO/T in the $NaAlSi_3O_8$–H_2O systems. The curves in (**a**) and (**c**) show the connecting lines for the 3000 K data in the corresponding systems. The lines in (**b**) and (**d**) show linear fits to the data at all temperatures. The open symbols in (**a**) and (**b**) are the FPMD results of the SiO_2–H_2O system with 23.1 wt% H_2O at 3000 K (Spiekermann et al., 2016). The larger open symbols in (**c**) and (**d**) are the FPMD results of the $NaAlSi_3O_8$ melt from Bajgain and Mookherjee (2020) at 2500 K (2.78 GPa) and 3000 K (3.31 GPa). The smaller open symbols in (**c**) and (**d**) are the FPMD results of anhydrous and hydrous (4.2 wt% H_2O) $NaAlSi_2O_6$ melt at 2500 K (3.21 GPa, 2.72 GPa) and 3000 K (2.28 GPa, 2.03 GPa) obtained by Bajgain et al. (2019).

Figure 3. Speciation of hydrogen in the (**a**) SiO_2–H_2O and (**b**) $NaAlSi_3O_8$–H_2O systems. The abundance of H_2O_m species = the number of H_2O_m species divided by the total number of all types of hydrogen species.

Figure 4. Water content and temperature dependence of the self-diffusion coefficients for Si, O and H in the SiO_2–H_2O systems. The FPMD results for hydrous (with 8.25 wt% H_2O) SiO_2 liquid (Karki and Stixrude, 2010) at 2500 K (~ 0 GPa), 3000 K (~ 4.08 GPa) and 3500 K (~ 0.61 GPa) are included for comparison.

Figure 5. Water content, and temperature dependence of the self-diffusion coefficients (*D*) for Na, Al, Si, O and H in the $NaAlSi_3O_8$–H_2O systems. The FPMD results of the $NaAlSi_3O_8$ melt

from Bajgain and Mookherjee (2020) at 2500 K (2.78 GPa) and 3000 K (3.31 GPa) and that from Kobsch and Caracas (2020) at 3000 K (~ 4.8 GPa) are included for comparison.

Figure 6. Viscosities of the SiO_2–H_2O and $NaAlSi_3O_8$–H_2O systems. The error bars indicate the mean absolute error. (**a**) The viscosities of the SiO_2–H_2O systems as a function of water content. The calculated viscosities (η) of the SiO_2–H_2O systems in this study at 2600 K (blue filled squares), 3000 K (red filled squares) and 3500 K (green filled squares) are shown. The FPMD results for hydrous (with 8.25 wt% H_2O) SiO_2 liquid (Karki and Stixrude, 2010) at 3000 K (~ 4.08 GPa) and 3500 K (~ 0.61 GPa) are included for comparison. (**b**) The viscosities of the $NaAlSi_3O_8$–H_2O systems as a function of water content. The calculated viscosities of the $NaAlSi_3O_8$–H_2O systems in this study at 2000 K (yellow filled circles), 2500 K (blue filled circles) and 3000 K (red filled circles) are shown. The FPMD results for the $NaAlSi_3O_8$ melt (Bajgain and Mookherjee, 2020) at 2500 K (2.78 GPa) and 3000 K (3.31 GPa) are included for comparison. The black dashed line and the blue dashed line show the results obtained from the experimental model of Audétat and Keppler (2004) at 2000 K and 2500 K, respectively. The insets show our viscosity data plotted with a linear y-axis. The corresponding stress ACF can be found in Figures S8 and S9 in Supporting Information.

Figure 7. Snapshot of the SiO_2–H_2O (left, 2600 K) and $NaAlSi_3O_8$–H_2O (right, 2000 K) systems with 50 wt% H_2O displayed by the 3D visualization program VESTA (Momma and Izumi, 2011). In addition to monomers, supercritical fluids contain various partially polymerized silicate units, including dimers, trimers and more polymerized species such as pentamers.

TABLES

Table 1. The calculated pressures of SiO_2–H_2O systems. The error bars are calculated using the method of Flyvbjerg and Petersen (1989).

H_2O (wt%)	System	Number of atoms	Pressure (GPa)		
			2600 K	3000 K	3500 K
0.00	60 SiO_2	180	—	3.14 ± 0.13	—
10.17	45 SiO_2 + 17 H_2O	186	3.25 ± 0.09	3.47 ± 0.09	3.65 ± 0.06
19.99	36 SiO_2 + 30 H_2O	198	3.49 ± 0.07	3.62 ± 0.08	4.07 ± 0.06
30.22	27 SiO_2 + 39 H_2O	198	3.25 ± 0.05	3.55 ± 0.05	4.03 ± 0.05
40.16	21 SiO_2 + 47 H_2O	204	3.24 ± 0.05	3.57 ± 0.06	4.02 ± 0.04
49.99	15 SiO_2 + 50 H_2O	195	3.24 ± 0.04	3.64 ± 0.05	4.12 ± 0.04
59.17	12 SiO_2 + 58 H_2O	210	—	3.57 ± 0.04	—
70.94	7 SiO_2 + 57 H_2O	192	—	3.66 ± 0.04	—

Table 2. The calculated pressures for the $NaAlSi_3O_8$–H_2O systems.

H_2O (wt%)	System	Number of atoms	Pressure (GPa)		
			2000 K	2500 K	3000 K
0.00	16 $NaAlSi_3O_8$	208	—	—	3.03 ± 0.09
10.27	12 $NaAlSi_3O_8$ + 20 H_2O	216	1.92 ± 0.07	2.57 ± 0.09	3.06 ± 0.07
20.49	8 $NaAlSi_3O_8$ + 30 H_2O	194	2.09 ± 0.07	2.50 ± 0.07	3.01 ± 0.05
30.04	8 $NaAlSi_3O_8$ + 50 H_2O	254	1.94 ± 0.06	2.47 ± 0.06	3.03 ± 0.05
40.72	4 $NaAlSi_3O_8$ + 40 H_2O	172	2.03 ± 0.06	2.52 ± 0.05	3.07 ± 0.05
50.75	4 $NaAlSi_3O_8$ + 60 H_2O	232	1.88 ± 0.04	2.41 ± 0.04	2.92 ± 0.04
60.18	4 $NaAlSi_3O_8$ + 88 H_2O	316	—	—	2.86 ± 0.04

FIGURES

This is the peer-reviewed, final accepted version for American Mineralogist, published by the Mineralogical Society of America.
The published version is subject to change. Cite as Authors (Year) Title. American Mineralogist, in press.
DOI: https://doi.org/10.2138/am-2022-8724. http://www.minsocam.org/

Figure 1

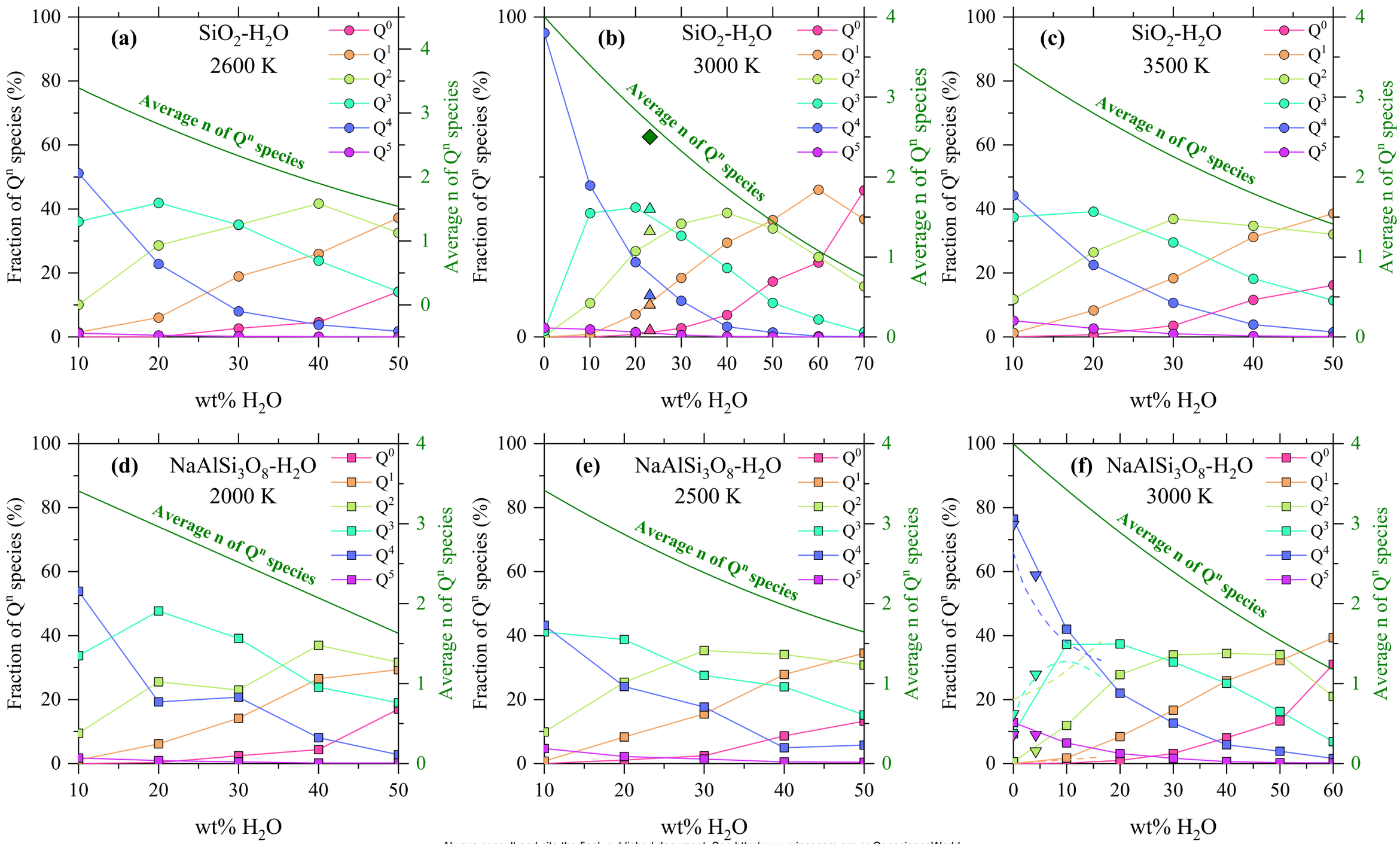

This is the peer-reviewed, final accepted version for American Mineralogist, published by the Mineralogical Society of America.
The published version is subject to change. Cite as Authors (Year) Title. American Mineralogist, in press.
DOI: https://doi.org/10.2138/am-2022-8724. http://www.minsocam.org/

Figure 2

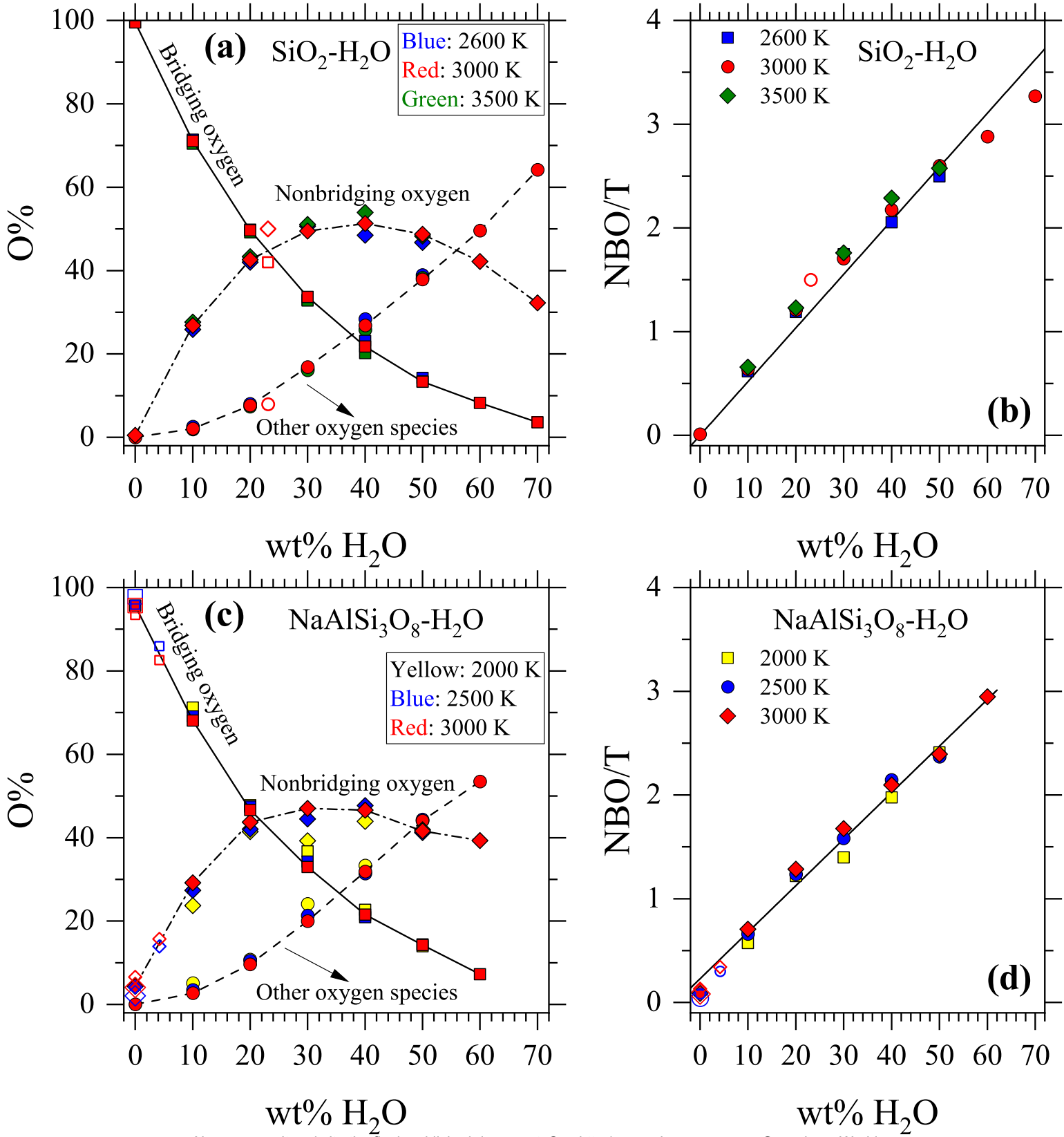

This is the peer-reviewed, final accepted version for American Mineralogist, published by the Mineralogical Society of America.
The published version is subject to change. Cite as Authors (Year) Title. American Mineralogist, in press.
DOI: https://doi.org/10.2138/am-2022-8724. http://www.minsocam.org/

Figure 3

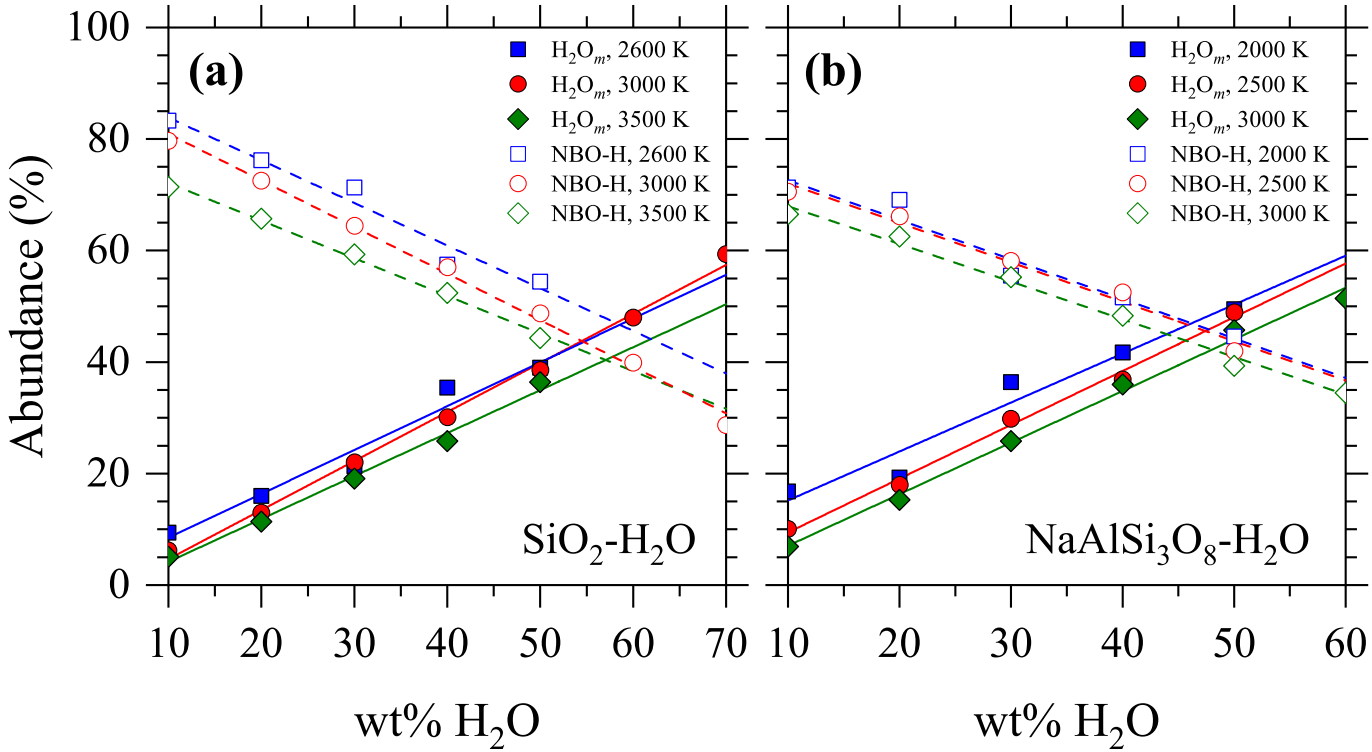

This is the peer-reviewed, final accepted version for American Mineralogist, published by the Mineralogical Society of America.
The published version is subject to change. Cite as Authors (Year) Title. American Mineralogist, in press.
DOI: https://doi.org/10.2138/am-2022-8724. http://www.minsocam.org/

Figure 4

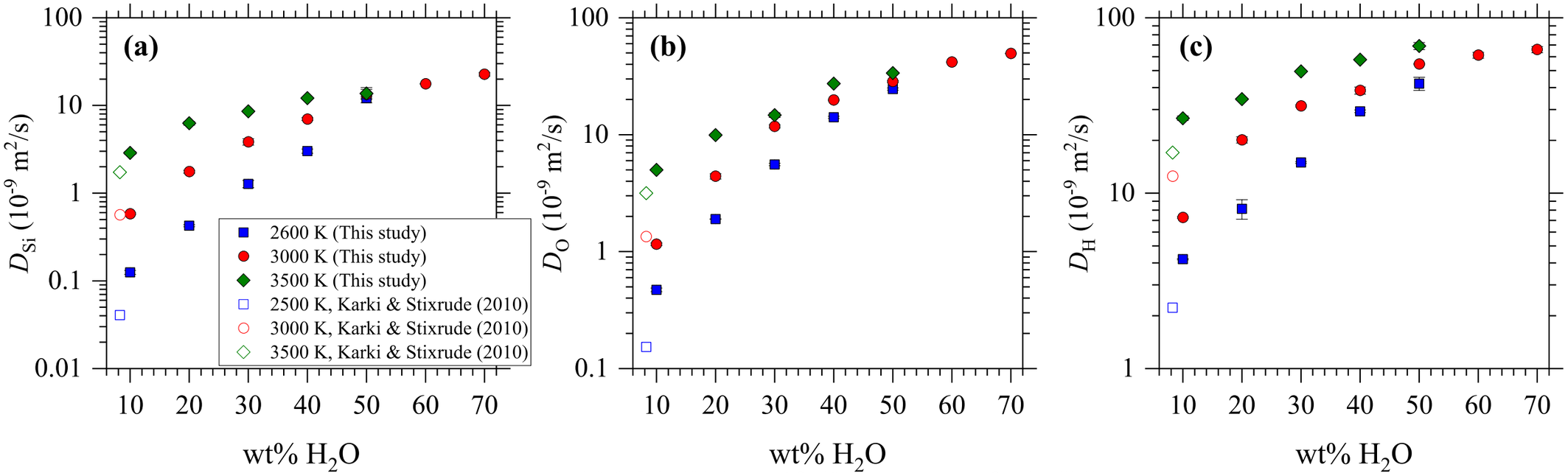

This is the peer-reviewed, final accepted version for American Mineralogist, published by the Mineralogical Society of America.
The published version is subject to change. Cite as Authors (Year) Title. American Mineralogist, in press.
DOI: https://doi.org/10.2138/am-2022-8724. http://www.minsocam.org/

Figure 5

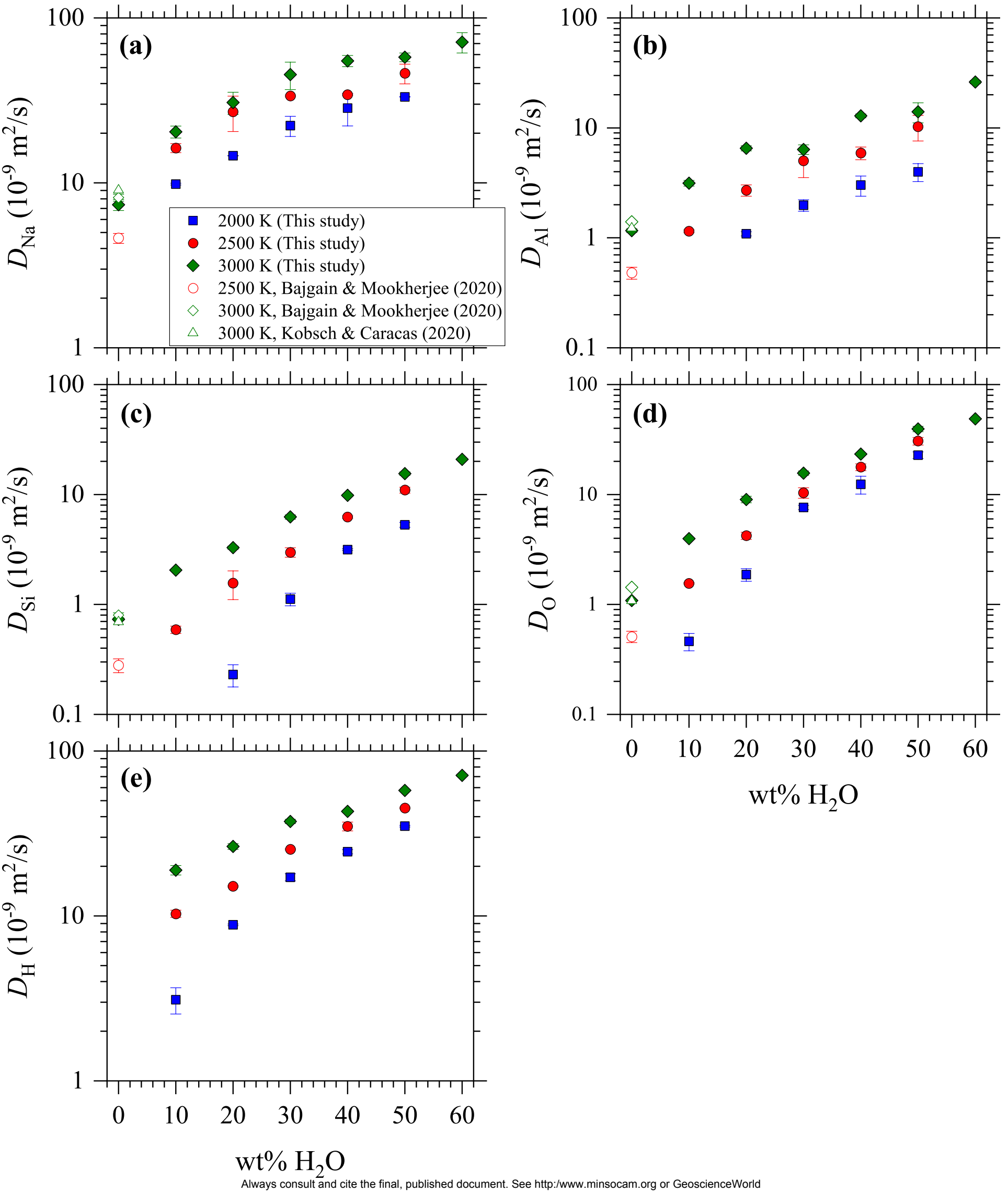

This is the peer-reviewed, final accepted version for American Mineralogist, published by the Mineralogical Society of America.
The published version is subject to change. Cite as Authors (Year) Title. American Mineralogist, in press.
DOI: https://doi.org/10.2138/am-2022-8724. http://www.minsocam.org/

Figure 6

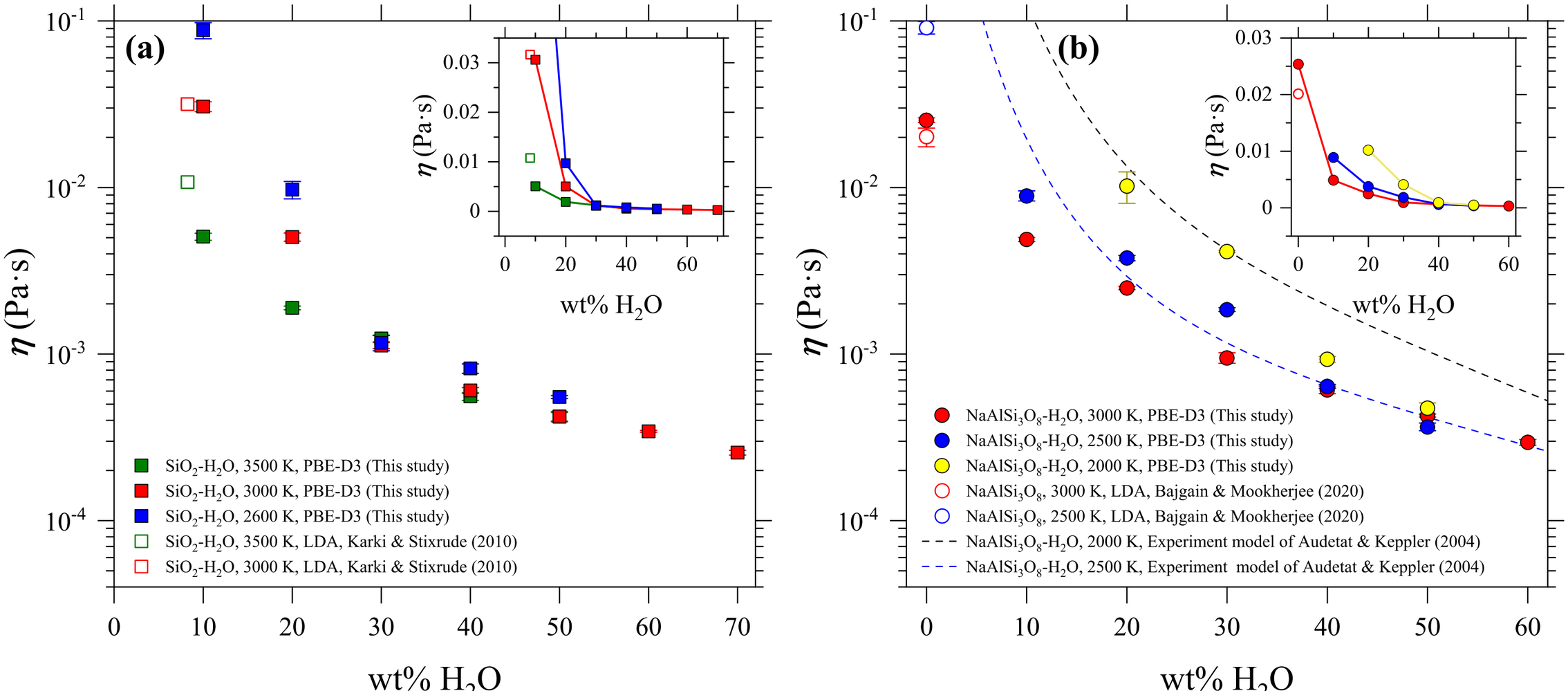

This is the peer-reviewed, final accepted version for American Mineralogist, published by the Mineralogical Society of America.
The published version is subject to change. Cite as Authors (Year) Title. American Mineralogist, in press.
DOI: https://doi.org/10.2138/am-2022-8724. http://www.minsocam.org/

Figure 7